Membrane microdomain switching: a regulatory mechanism of amyloid precursor protein processing

Takashi Sakurai,[1,2,4] Kumi Kaneko,[1,2] Misako Okuno,[1,2] Koji Wada,[1] Taku Kashiyama,[1,4] Hideaki Shimizu,[1] Takumi Akagi,[3] Tsutomu Hashikawa,[3] and Nobuyuki Nukina[1,2]

[1]Laboratory for Structural Neuropathology, [2]Laboratory for Neurodegeneration Signal, and [3]Laboratory for Neural Architecture, RIKEN Brain Science Institute, Wako, Saitama 351-0198, Japan
[4]Department of Pharmacology, Juntendo University School of Medicine, Bunkyo-ku, Tokyo 113-8421, Japan

Neuronal activity has an impact on β cleavage of amyloid precursor protein (APP) by BACE1 to generate amyloid-β peptide (Aβ). However, the molecular mechanisms underlying this effect remain to be elucidated. Cholesterol dependency of β cleavage prompted us to analyze immunoisolated APP-containing detergent-resistant membranes from rodent brains. We found syntaxin 1 as a key molecule for activity-dependent regulation of APP processing in cholesterol-dependent microdomains. In living cells, APP associates with syntaxin 1–containing microdomains through X11–Munc18, which inhibits the APP–BACE1 interaction and β cleavage via microdomain segregation. Phosphorylation of Munc18 by cdk5 causes a shift of APP to BACE1-containing microdomains. Neuronal hyperactivity, implicated in Aβ overproduction, promotes the switching of APP microdomain association as well as β cleavage in a partially cdk5-dependent manner. We propose that microdomain switching is a mechanism of cholesterol- and activity-dependent regulation of APP processing in neurons.

Introduction

Increasing evidence indicates that amyloid-β peptide (Aβ) plays a central role in the pathogenesis of Alzheimer's disease (AD; Selkoe and Schenk, 2003). Aβ is generated by sequential cleavage of amyloid precursor protein (APP) by β-secretase (BACE1; Vassar et al., 1999) and γ-secretase, whereas alternative cleavage by α-secretase precludes Aβ production (De Strooper and Annaert, 2000). It is of critical importance to determine how these alternative cleavages are regulated. In vitro and in vivo studies (Simons et al., 1998; Refolo et al., 2000; Fassbender et al., 2001) have shown that high cellular cholesterol levels promote β cleavage and Aβ generation. A recent study indicates that Aβ regulates cholesterol metabolism, suggesting that cholesterol dependency of β cleavage may be part of the feedback system for cholesterol homeostasis (Grimm et al., 2005). BACE1 associates with cholesterol-dependent membrane microdomains,

lipid rafts (Riddell et al., 2001). Because a fraction of APP shows cholesterol-dependent association with lipid rafts (Simons et al., 1998), rafts have been postulated to be a critical site for β cleavage and cholesterol-dependent regulation of APP–BACE1 interaction. Association of α-secretase with nonraft domains may also contribute to the cholesterol dependency (Kojro et al., 2001). However, a paradoxical acceleration of β cleavage by a slight reduction in cellular cholesterol levels (Abad-Rodriguez et al., 2004) might point to a limitation of the alternative association model of APP with rafts or nonrafts for explaining cholesterol-dependent regulation of β/α cleavage (Wolozin, 2001).

APP is anterogradely transported in axons and may contribute to neurite outgrowth and synaptogenesis in neurons (Reinhard et al., 2005). After exposure on the cell surface, APP undergoes a rapid turnover by α-secretase at the cell surface or by BACE1 after endocytosis (Nixon, 2005; Cirrito et al., 2008). The cytoplasmic C-terminal domain of APP plays critical roles in its trafficking and processing by binding to adaptor proteins, including Fe65 and X11 family proteins

The Rockefeller University Press $30.00
J. Cell Biol. Vol. 183 No. 2 339–352
www.jcb.org/cgi/doi/10.1083/jcb.200804075

JCB 339

(King and Turner, 2004). Overexpression of X11 or X11L, which are predominantly expressed in neurons, suppresses APP processing and Aβ generation in HEK293 cells (Borg et al., 1998). Munc18, an X11/X11L-interacting protein, synergistically accelerates the inhibitory effects of X11 on APP processing through direct and indirect functional interactions between X11 and Munc18 in HEK293 cells (Ho et al., 2002). Neither the precise mechanism nor the effect of Munc18 on APP processing in neurons has been elucidated. X11 but not X11L interacts with calcium/calmodulin-dependent serine protein kinase (CASK)-Veli to form an evolutionarily conserved heterotrimeric complex involved in the targeting of receptors in polarized cells (King and Turner, 2004). Contrary to cell culture models, no significant change in the levels of APP and its metabolites was observed in X11-null mice (Ho et al., 2003).

Neuronal/synaptic activity is known as an important regulator of β cleavage (Kamenetz et al., 2003). In this connection, new types of microdomains related to exocytotic SNAREs may be of importance. Syntaxin 1, which is involved in synaptic vesicle docking/fusion under the control of Munc18, is associated with cholesterol-dependent microdomains but is segregated from Thy-1, a glycosyl-phosphatidylinositol (GPI)–anchored typical raft resident (Lang et al., 2001). A structural change in syntaxin 1 from a closed to an open conformation induced by phosphorylation of Munc18 by cdk5 may promote core complex formation essential for exocytosis (Rizo and Sudhof, 2002). A broad spectrum of substrates, including Munc18 (Fletcher et al., 1999) and APP (Iijima et al., 2000), suggests the involvement of cdk5 in the coordination of vesicle trafficking (Smith and Tsai, 2002). Cdk5 is active on the plasma membrane or cell periphery as a complex with p35, an essential activator with a membrane anchor at the N terminus. Ectopic hyperactivity of cdk5 caused by cleavage of p35 to p25 has been implicated in AD (Nguyen et al., 2002; Smith and Tsai, 2002) and promotion of Aβ production (Cruz et al., 2006). These results may indicate convergence of the two important regulatory mechanisms of Aβ production, neuronal/synaptic activity and cellular cholesterol levels, on specific membrane microdomains.

We aimed to characterize APP-containing microdomains to understand the mode of cholesterol-dependent microdomain association of APP and neuronal activity–dependent regulation of β cleavage. Our analyses indicate a preferential association of APP with syntaxin 1–containing microdomains and segregation from BACE1-containing microdomains. Dissociation of the X11–Munc18–syntaxin 1 interaction induced a shift in APP association from syntaxin- to BACE1-containing microdomains and promotion of β cleavage. We also found that neuronal hyperactivity promoted the shift in microdomain association of APP and β cleavage in a partially cdk5-dependent manner. We propose that microdomain switching, the alternative association of APP with syntaxin 1–containing microdomains via X11–Munc18–syntaxin 1 or with BACE1-containing microdomains induced by dissociation from syntaxin 1, is a novel regulatory mechanism of an activity-dependent increase in β cleavage in neurons.

Results

Characterization of detergent-resistant membrane (DRM) fractions isolated with Lubrol WX

Biochemically, membrane microdomains are characterized as DRMs by insolubility in nonionic detergents at 4°C and flotation on density gradients. Triton X-100 is the standard detergent for this purpose, but other detergents are also useful for showing microdomain heterogeneity or other types of microdomains (Madore et al., 1999; Roper et al., 2000; Pike, 2004). We prepared DRMs for two main purposes: (1) the efficient and reproducible recovery of APP in DRMs from brains and (2) to maintain the separate identity of membranes without substantial intermingling of protein components to validate immunoaffinity purification. We tried several nonionic detergents, including Brij 97 and Lubrol WX. All detergents tested showed a clear enrichment of a DRM marker, prion protein (PrP), in DRM fractions and separation from a detergent-soluble membrane marker, calnexin (Fig. 1 a). DRM fractions were also rich in cholesterol and GM1-ganglioside (unpublished data).

By Western blot (WB) analysis, Triton X-100 and Brij showed variable (poor in most cases) recovery of APP in DRMs. In contrast, a substantial part of APP was found in DRMs isolated with Lubrol. Interestingly, Lubrol caused an enrichment of the mature forms of APP (late Golgi or post-Golgi forms) in DRMs and recovery of the immature form (an ER or early Golgi form) mainly in the detergent-soluble fractions. This differential solubilization might reflect the formation of a mature Lubrol-resistant microdomain during transport across the Golgi. Quantitative measurements confirmed that the majority of mature APP was resistant to solubilization with Lubrol but not with Brij (Fig. 1 b). This differential solubilization of APP was also observed in DRMs derived from primary neurons (Fig. 1 c). With Lubrol, a substantial part of mature BACE1 was consistently recovered in the DRM fractions (Riddell et al., 2001). In contrast, ADAM17, a putative α-secretase, showed solubility with Lubrol.

We checked the levels of membrane mixing induced by Lubrol by using a DRM preparation from a cohomogenized mixture of mouse and rat brain tissues followed by immunoprecipitation (IP) with species-specific anti–Thy-1 antibodies (Madore et al., 1999). Because Madore et al. (1999) had already demonstrated intermingling of Thy-1 in DRMs prepared by Triton X-100, we focused on Brij and Lubrol. WB analysis of DRM fractions derived from brain tissues demonstrated negligible levels of Thy-1 mixing in the case of Lubrol WX, whereas Brij 97 showed detectable levels (Fig. 1 d). These results demonstrate the superiority of Lubrol WX for analyzing APP-rich microdomains and suggest that Lubrol maintains the separate identities of membranes to validate immunoisolation.

To test the feasibility of the immunoisolation of DRMs, we checked the distribution of APP on Lubrol DRMs. First, we checked the morphology of DRMs by EM (Fig. S1, a and b, available at http://www.jcb.org/cgi/content/full/jcb.200804075/DC1). Triton X-100 DRMs showed vesicular structures as described previously (Roper et al., 2000), which is consistent with robust membrane mixing (Madore et al., 1999). However, Lubrol DRMs
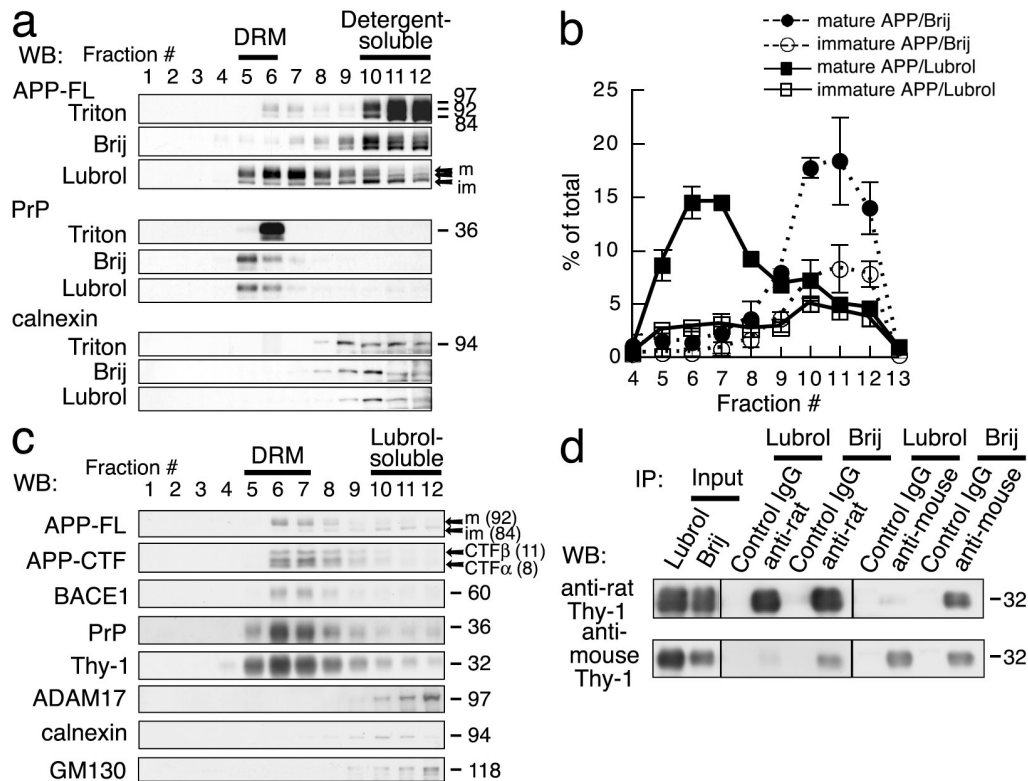
Figure 1. **Mature forms of APP and BACE1 show association with Lubrol-resistant membranes.** (a) Mature forms of APP were efficiently recovered in DRM fractions derived from mouse brains solubilized with Lubrol WX but poorly with Triton X-100 or Brij 97. All three detergents showed recovery of PrP (a DRM marker) in DRM fractions well separated from calnexin (a detergent-soluble membrane marker). Arrows, different forms of FL-APP; m, mature forms; im, immature form of APP. (b) Quantitative comparison of distributions of mature and immature forms of APP across the gradients after Lubrol WX or Brij 97 solubilization. Each point represents a percentage of the total. Results are mean ± SD based on three to four independent experiments. (c) Mature forms and CTFs of APP and BACE1 associate with DRM fractions derived from primary cultured cortical neurons solubilized with Lubrol WX, whereas ADAM17 mainly resides in Lubrol-soluble membranes. GPI-anchored proteins Thy-1 and PrP were used as DRM markers, and calnexin and GM130 were used as detergent-soluble membrane markers. We used longer exposure to detect APP-CTFs compared with FL-APP. (d) Lubrol WX causes only negligible levels of artifactual intermingling of Thy-1. Rat and mouse brain tissues were cohomogenized in 1% Lubrol WX or 1% Brij 97, and DRMs were prepared. Thy-1 on DRMs was immunoaffinity purified and probed with species-specific antibodies. Lubrol caused only negligible levels of mixing of Thy-1 on DRMs during solubilization, centrifugation, and immunoisolation.

showed various shapes and sizes of sheetlike structures. Next, DRMs were stained with anti-APP and gold-labeled secondary antibody and observed by EM (Fig. S1, c and d). Gold particles were visualized as clusters on significantly smaller numbers of membrane structures than expected from a random distribution (Poisson distribution, x^2 test, P < 0.001, n = 255), suggesting an accumulation of APP in specific subpopulations of Lubrol DRMs.

### Immunoisolation of APP-containing DRM subfractions

To analyze APP-rich Lubrol-DRM subfractions derived from brain tissue or primary neurons, we performed immunomagnetic isolation using an affinity-purified antibody against the APP cytoplasmic domain. Successful isolation was shown by WB analysis, demonstrating almost complete precipitation of APP in DRMs (Fig. 2 b) and blocking by antigen peptide preabsorption (not depicted). The anti-APP antibody precipitated a discrete set of proteins from the input DRMs (Fig. 2 a) corresponding to 2% of the total input (estimation by SYPRO Ruby staining), indicating an association of APP with specialized subpopulations of DRMs. Identification of protein components by mass spectrometry (MS) and WB analysis revealed syntaxin 1 as a

probable link between APP and the cholesterol-dependent microdomains distinct from rafts (Lang et al., 2001) and a possible connection with synaptic activity. As candidate links between APP and syntaxin 1, X11/X11L and Munc18 were detected in APP-containing DRMs by WB (Fig. 2 b) but not by MS analysis. Because APP–X11–Munc18 and X11–Munc18–syntaxin 1 interactions have been reported, we hypothesized that X11/X11L–Munc18 provides a link between APP and syntaxin 1.

Characterization of APP-containing DRM subfractions

To characterize the organization of APP DRMs, we treated them with 60 mM octylglucoside (OG), an effective detergent for solubilizing raft proteins, at RT. Next, we size fractionated the protein complexes in a glycerol gradient. APP, Munc18, and syntaxin 1 showed broad distribution across the gradient in contrast to BACE1 (see Fig. S2 a, available at http://www.jcb.org/cgi/content/full/jcb.200804075/DC1). Fractions corresponding to ~6,000 kD lacking BACE1 were used for further immunoisolation with anti-APP. The bound fraction contained proteins such as Munc18, syntaxin 1, and CASK, suggesting an involvement of X11–Munc18–syntaxin 1 in the large APP complex.

Figure 2. **Successful immunoisolation of DRM subfractions rich in APP or BACE1.** Protein compositions of immunoisolated DRM subfractions were compared by silver staining (a) and WB (b). Brain-derived Lubrol DRMs were immunoaffinity purified with anti-APPc or anti-BACE1c. Protein band patterns of the DRM subfractions were distinct from that of the input (a). WB analysis showed minimal overlap between APP and BACE1 (b). X11, CASK, Munc18, and syntaxin 1 were enriched in APP DRMs. Proteins in the bound fraction derived from the same amount of DRM were loaded. The total amount of bound proteins in BACE1 DRMs estimated by SYPRO Ruby staining was roughly 50% of that in APP DRMs. PrP showed preferential association with APP DRMs over BACE1 DRMs.
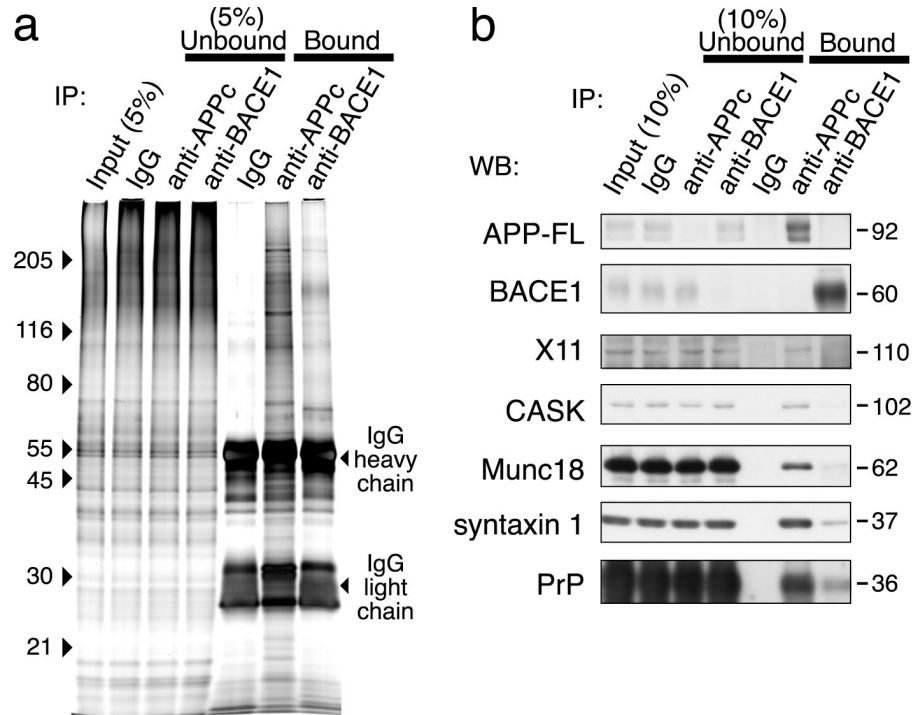
Cholesterol depletion by methyl-β-cyclodextrin (MβCD) and subsequent cholesterol replenishment with a preformed cholesterol–MβCD complex has been used to show cholesterol-dependent microdomain association (Simons and Toomre, 2000). MβCD treatment caused a partial shift of full-length (FL) APP into heavier fractions that was reversed by cholesterol replenishment, indicating a cholesterol-dependent DRM association of APP as well as BACE1 (Fig. S2 b). A fraction of X11/X11L and CASK was associated with DRMs (Fig. S2 b for X11 and CASK), suggesting binding of these proteins to integral membrane proteins in DRMs. Association of X11 and CASK with DRMs showed cholesterol dependence, whereas that of Munc18 and syntaxin 1 was less clear. Because X11L demonstrated somewhat variable results in cholesterol dependency, we focused on X11 and CASK in subsequent experiments.

To exclude the possibility that accumulation of the identified proteins was the result of artifactual changes caused by detergent solubilization, we adopted a detergent-free preparation of DRM-like membranes followed by immunoisolation (Vetrivel et al., 2004). WB analysis of APP-rich membranes derived from cortical neurons showed coresidence of the same proteins in DRM-like membranes (Fig. S3, available at http://www.jcb.org/cgi/content/full/jcb.200804075/DC1).

BACE1 is largely excluded from APP-containing DRMs

To study the involvement of syntaxin 1 in the APP–BACE1 interaction, we isolated DRMs rich in BACE1 (Fig. 2 b). Interestingly, APP and BACE1 showed only minimal overlap between DRM subfractions. To exclude the possibility that APP cleavage by BACE1 reduced coresidence, we used a membrane-permeable β-secretase inhibitor (Stachel et al., 2004) for DRM preparation from cortical neurons and immunoisolation. Even in this situation,

overlap between APP and BACE1 was minimal (unpublished data). Consistently, X11, Munc18, and syntaxin 1 were detected only at low levels in the BACE1 DRMs. PrP was relatively enriched in APP-containing DRMs. These results suggest an exclusion of BACE1 from APP-containing complexes in DRMs.

APP and BACE1 associate with distinct microdomains in neurons

In living cells, Thy-1 segregates away from PrP (Madore et al., 1999) and syntaxin 1 clusters (Lang et al., 2001) but associates with BACE1 in microdomains (Abad-Rodriguez et al., 2004). Conversely, APP segregates away from BACE1 in copatching experiments on primary neurons (Abad-Rodriguez et al., 2004) and in our DRM analysis but shows a preferential association with syntaxin 1 and PrP in DRMs (Fig. 2 b). These results prompted us to study the relationship between APP and microdomains rich in Thy-1 or PrP. These two GPI-anchored proteins are useful markers to analyze distinct microdomains in living neurons (Madore et al., 1999). We performed copatching of endogenous cell surface proteins on living hippocampal neurons as an established method to observe coresidence in the same microdomains (Harder et al., 1998; Abad-Rodriguez et al., 2004). To visualize antibody-induced protein clusters (patches) on the cell surface, we incubated live cells with two different sets of primary and fluorescently labeled secondary antibodies. Overlap between clusters of different proteins would indicate coresidence in the same microdomain. On primary neurons, patching of endogenous proteins revealed relative segregation between Thy-1 and APP as well as a preferential association between PrP and APP (Fig. 3, a and b). Exogenously expressed BACE1 showed a preferential association with Thy-1 and segregation from APP, as described previously (Abad-Rodriguez et al., 2004), and PrP (unpublished data). These results consistently indicate

an association between PrP and APP and between Thy-1 and BACE1 as well as segregation of these two groups.

To investigate the molecular mechanisms underlying these specific microdomain associations and their involvement in β cleavage, we used N2a cells that endogenously express proteins enriched in neurons, such as X11, Munc18-1, and syntaxin 1. To perform copatching experiments, we transiently expressed minimum levels of proteins for patch detection. This was because the expression levels of X11 and Munc18-1 in N2a cells are low compared with neurons and because high-level expression of APP would saturate the binding sites and cause mislocalization of APP. For detecting syntaxin 1 clusters on the surface of the cell, we used syntaxin 1 fused with an HA tag through a flexible linker (Mitchell and Ryan, 2004) at the C terminus (syntaxin 1–HA), which was expressed at comparable levels to endogenous syntaxin 1 (Fig. S4, available at http://www.jcb.org/cgi/content/full/jcb.200804075/DC1). Sequential incubation with primary and secondary antibodies induced the redistribution of surface-exposed proteins to form large-scale patches on the cell surface (Fig. S5). Copatching experiments in N2a cells corroborated the results obtained with primary neurons (Fig. 3, c and d). Syntaxin patches showed preferential colocalization with APP and PrP and segregation from BACE1.

X11–Munc18 interaction regulates association of APP with syntaxin 1–containing microdomains and segregation from BACE1

Because X11 is one of the most probable candidates for APP's association with syntaxin 1–containing microdomains, we tested the ability of truncated X11 mutants to disrupt APP–syntaxin 1 copatching by preventing the endogenous APP–X11 interaction (Fig. 4 a). Overexpression of functional domains in X11 (Mueller et al., 2000) showed diminished association of binding partners in N2a cells (Fig. 4 c). Interestingly, APP–syntaxin 1 copatching was significantly reduced by overexpression of the Munc18 interaction domain (MID) or MID–CASK-interacting domain (CID) but not by CID alone, indicating the involvement of an X11–Munc18 interaction in the association of APP with syntaxin 1–containing microdomains.

To directly test the APP–BACE1 interaction on N2a cells, we performed APP–BACE1 copatching experiments using a BACE1 mutant defective in endocytosis (BACE1AA; see Materials and methods and Fig. S5). Control cells showed relatively low levels of APP–BACE1 copatching (Fig. 4 a), which is consistent with a previous study (Abad-Rodriguez et al., 2004) and our DRM analysis (Fig. 2). MID-expressing cells demonstrated an increase in APP–BACE1 copatching, suggesting an inhibitory effect of X11–Munc18 on the APP–BACE1 interaction. However, MID–CID abolished the effect of MID on the APP–BACE1 interaction. Consistently, CID slightly reduced APP–BACE1 copatching. These results imply a positive role of CID on the APP–BACE1 interaction and an elaborate regulatory mechanism through X11.

Next, we studied the effects of X11 on β cleavage by endogenous BACE1 (Fig. 4 b). Because X11 has been reported to be involved in γ-cleavage (Xie et al., 2005), we measured the released extracellular domain by α and β cleavage in the medium, secreted
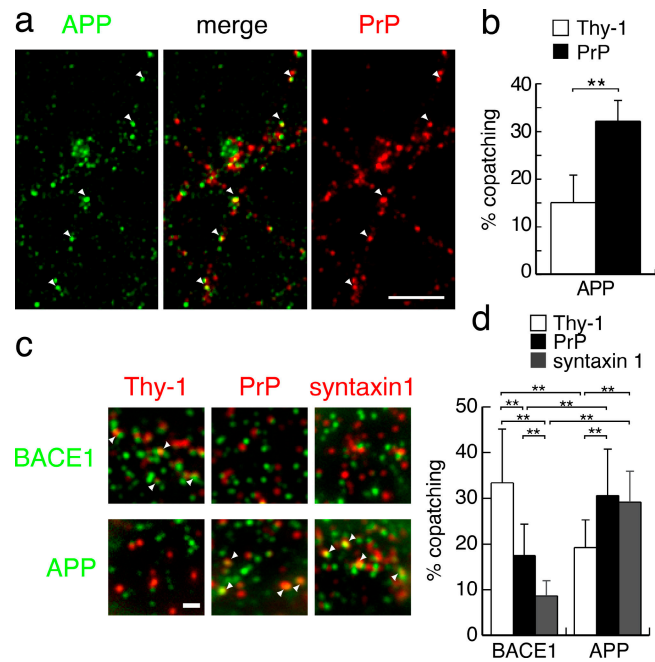
Figure 3. **Copatching demonstrates a preferential association between APP and PrP and BACE1 and Thy-1 as well as the relative separation between these two groups.** (a) Preferential copatching between endogenous APP and PrP on axons of primary neurons. Mouse hippocampal neurons were treated with rabbit anti-APPex and rat anti–Thy-1.2 or mouse anti-PrP followed by fluorescently labeled secondary antibodies to induce patches of endogenous proteins on neurons. Colocalized APP and PrP patches are indicated by arrowheads. Bar, 5 µm. (b) Quantitative measurements of copatching demonstrated a statistically significant difference between APP–PrP and APP–Thy-1. $n = 60$. (c and d) Copatching on N2a cells demonstrates a preferential association between APP and PrP or syntaxin 1–HA and BACE1 and Thy-1 as well as the relative separation between these two groups. (c) Copatching is indicated by arrowheads. Bar, 1 µm. Quantitative measurements are shown in panel d. $n = 34$–44. (b and d) Data are means + SD based on three independent experiments. **, $P < 0.01$.

APPα (sAPPα) and sAPPβ, by using C-terminal end-specific antibodies. Because α and β cleavages are mutually exclusive, we used the ratio of sAPPβ to sAPPα as an indicator. MID overexpression in N2a cells caused an increase in sAPPβ/sAPPα, suggesting an inhibitory effect of X11–Munc18 against β cleavage. However, MID–CID expression has no effect on β cleavage, and CID decreased β cleavage, suggesting a positive role of CID on β cleavage. CASK may be one of the candidates mediating this activity.

To confirm the requirement of Munc18 for microdomain association of APP and β cleavage regulation, we analyzed the effects of RNAi-mediated knockdown of Munc18 (Fig. 5). Ablation of Munc18 reduced the association of syntaxin 1 with APP observed by co-IP (Fig. 5 c). Reduction of APP–syntaxin 1 copatching (Fig. 5 a) confirmed the requirement of Munc18 for APP's association with syntaxin 1 microdomains. An increase in β cleavage (Fig. 5 b) was consistent with the negative regulation of β cleavage via X11–Munc18.

Cdk5 phosphorylation switches APP copatching from syntaxin 1 to BACE1

Phosphorylation of Munc18 by cdk5 is reported to induce conformational changes in syntaxin 1 to facilitate SNARE complex formation, although its physiological role is not yet elucidated
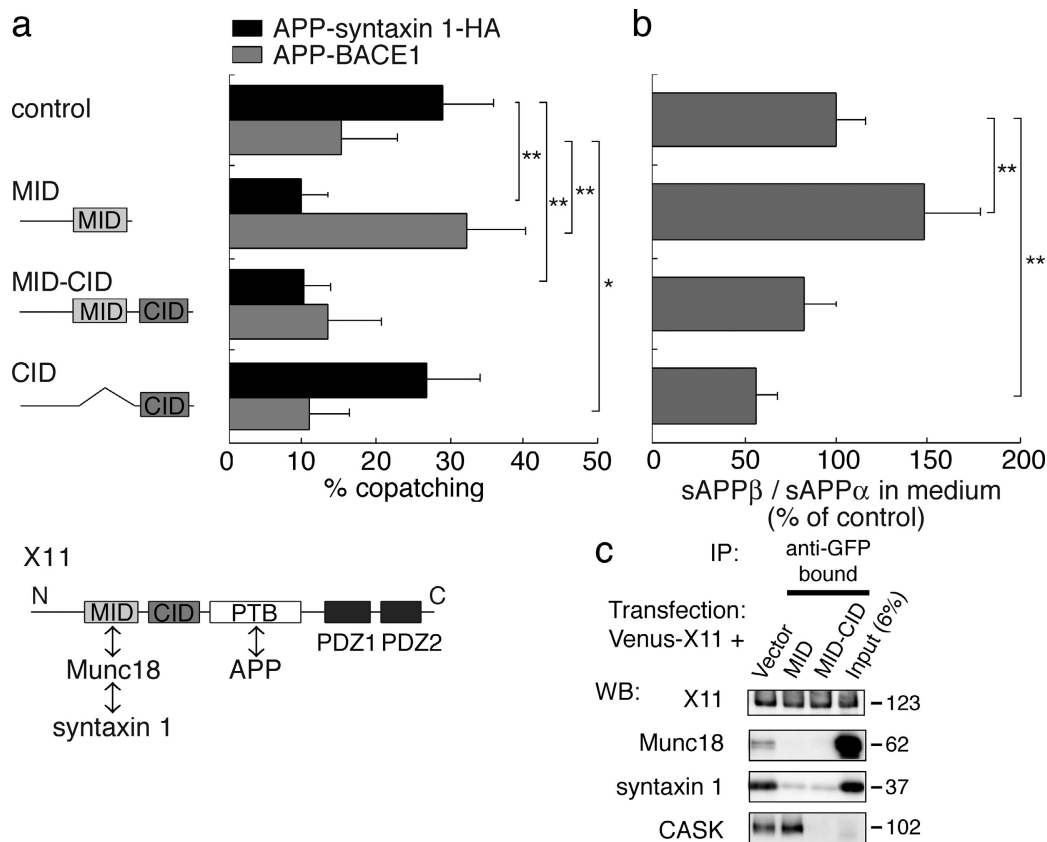
Figure 4. **X11–Munc18 regulates APP–BACE1 interaction and β cleavage in N2a cells.** (a) Effects of truncated X11 mutants on APP–syntaxin 1 and APP–BACE1 copatching. X11 interacts with Munc18–syntaxin 1 through MID and APP through the phosphotyrosine-binding domain. MID expression reduced APP–syntaxin 1, suggesting a requirement of X11–Munc18 for APP–syntaxin 1 copatching. APP–BACE1 copatching was promoted by MID and inhibited by CID, suggesting an inhibitory effect of Munc18 and a positive role of CID on the APP–BACE1 interaction. Copatching values were normalized against the control without X11 mutant expression. Error bars represent the SD based on three independent experiments ($n = 30–45$). (b) Effects of truncated X11 mutants on α/β cleavage. The extracellular domain of VSVG-tagged APP released into the medium by endogenous BACE1 or α-secretase was precipitated with anti-VSVG and quantified with end-specific antibodies. The effects of X11 mutants on β cleavage were consistent with their effects on APP–BACE1 interaction as shown in panel a. Ratios of sAPPβ to sAPPα were normalized against the control without X11 mutant expression. Data are means + SD based on three to four independent experiments ($n = 9$ or 12). (c) Effects of truncated mutants of X11 on interactions between X11 and Munc18 in N2a cells. The effects of MID and MID–CID on protein interactions were tested by co-IP analysis. Venus-X11 with MID or MID–CID was expressed, and the cell lysate was used for IP with anti-GFP. The X11–Munc18–syntaxin 1 interaction was diminished by MID and MID–CID, and the X11–CASK interaction was abolished by MID–CID. *, $P < 0.05$; **, $P < 0.01$.

(Fletcher et al., 1999; Rizo and Sudhof, 2002). We tested the effect of cdk5 on APP's microdomain association as a possible modulator. Because co-IP experiments demonstrated more efficient dissociation of APP, X11, and Munc18 from syntaxin 1 by cdk5/p35 (Fig. 6 c) than by cdk5/p25 (not depicted), we used cdk5/p35 for our subsequent experiments. Expression of cdk5/p35 in N2a cells caused a reduction of APP–syntaxin 1 copatching and a simultaneous increase in APP–BACE1 copatching (Fig. 6 a). To address whether the switching is mediated through Munc18 phosphorylation by cdk5, we used phosphorylation site mutants of Munc18, phosphorylation-resistant T574A that maintains affinity to syntaxin 1 (Fletcher et al., 1999), and a phosphorylation-mimetic T574E with reduced affinity to syntaxin 1 (Fig. 6 b; Liu et al., 2004). T574A blocked the effect of cdk5 on APP copatching, whereas T574E facilitated APP–BACE1 copatching and reduced APP–syntaxin 1 copatching without cdk5 expression. These results demonstrate that the effect of cdk5 is largely mediated by Munc18. Importantly, these data also indicate a requirement of syntaxin 1 for preventing the

APP–BACE1 interaction. Copatching experiments showed segregation between BACE1 and syntaxin 1 and association between PrP and syntaxin 1 regardless of cdk5 expression (unpublished data). Similarly, we tested the effect of a phosphorylation-resistant mutant of APP, T668A, which maintains affinity to X11 but reduces the association with Fe65 (Ando et al., 2001). This mutant did not affect APP–syntaxin 1 or APP–BACE1 copatching or cdk5-induced switching, suggesting a major role of X11–Munc18–syntaxin 1 in the cdk5-dependent regulation of APP–BACE1 interaction (unpublished data). Consistent with these results, there was no significant change in APP processing in APP T668A knock-in mice (Sano et al., 2006).

Association of APP with syntaxin 1–containing microdomains is involved in the regulation of APP–BACE1 interaction through microdomain segregation

To gain insight into the mechanism of BACE1 exclusion by syntaxin 1, we examined the effect of cholesterol depletion on
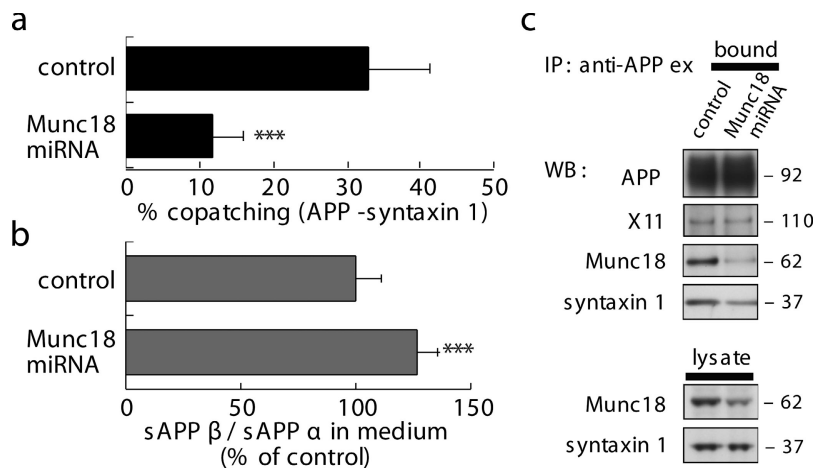
Figure 5. Munc18 is required for APP–syntaxin 1 co-patching and regulates β cleavage in N2a cells. (a) The effect of RNAi-mediated knockdown of endogenous Munc18 on APP–syntaxin 1 copatching. RNAi reduced APP–syntaxin 1 copatching, indicating a requirement of Munc18 for APP–syntaxin 1 copatching. Results are means + SD of 32–38 measurements. (b) The effect of Munc18 knockdown on β cleavage. N2a cells were transfected with pHVenus-APP and RNAi vector. Released sAPP in medium was captured with anti-GFP and quantified with anti-sAPP end-specific antibodies. Munc18 knockdown promoted β cleavage, which is consistent with an inhibitory role of X11–Munc18–syntaxin 1 on β cleavage. Data are means + SD based on four independent experiments ($n = 8$). (c) The effect of Munc18 knockdown on the interaction between APP and syntaxin 1. N2a cells were lyzed with Lubrol and used for IP with anti-APPex. In the lysate of N2a cells transfected with RNAi vector, syntaxin 1 association with APP was reduced. ***, $P < 0.001$.

BACE1–syntaxin 1 segregation (Fig. 7). Mild reduction of cellular cholesterol levels (Abad-Rodriguez et al., 2004) caused a shift in microdomain association of APP from syntaxin 1 to BACE1, whereas BACE1 and syntaxin 1 remained segregated. These changes are consistent with the failure of APP–X11–Munc18–syntaxin 1 complex formation demonstrated by the DRM analysis of cholesterol-depleted primary neurons (Fig. S2 b), probably because of the defective recruitment of APP into syntaxin 1 microdomains and subsequent stabilization by X11–Munc18. Further cholesterol depletion induced diminution of BACE1–syntaxin 1 segregation, indicating the requirement of intact cholesterol-dependent microdomains for BACE1–syntaxin 1 segregation.

Neuronal hyperactivity induces switching of APP microdomain association and increase in β cleavage

A recent study has implicated prolonged hyperactivity of cdk5 caused by p25 in the enhanced Aβ generation in neurons (Cruz et al., 2006). Although modulations in axonal transport or BACE1 protein levels (Wen et al., 2008) were suggested as possible mechanisms, microdomain switching may also be involved. We tested the effects of p25-induced cdk5 activation on microdomain association of APP in primary cultured neurons (Fig. 8). On axons of transfected neurons with APP, syntaxin 1–HA, and BACE1AA, we observed preferential copatching between APP
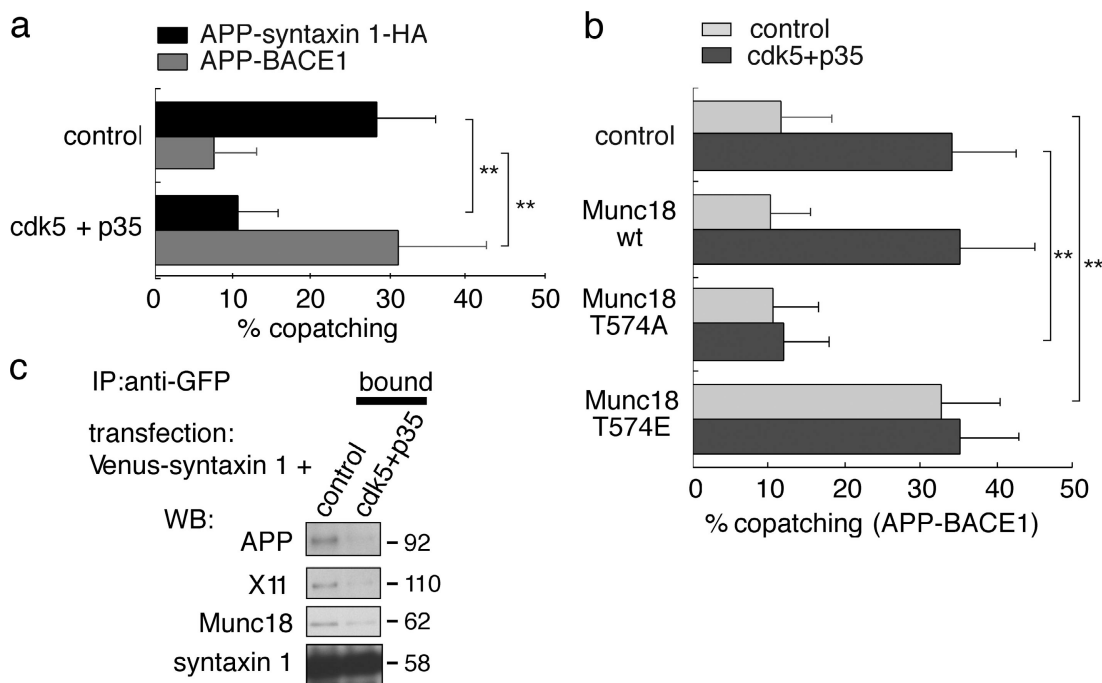

Figure 6. Association of APP with the syntaxin 1 microdomain through X11–Munc18 is controlled by cdk5 in N2a cells. (a) The effect of cdk5 on APP–syntaxin 1 and APP–BACE1 copatching. Cdk5/p35 expression caused switching of APP association in copatching. Results are means + SD of 20–31 measurements. (b) Effects of Munc18-1 mutants at the cdk5 phosphorylation site on APP–BACE1 copatching. Phosphorylation-resistant Munc18-1 T574A abolished the effect of cdk5, suggesting that the effect of cdk5 is mainly mediated by Munc18-1. A phosphorylation-mimetic mutant with reduced affinity to syntaxin 1, Munc18-1 T574E, had an effect similar to cdk5, indicating an involvement of syntaxin 1 and Munc18 in the regulation of the APP–BACE1 interaction. Data are means + SD based on three independent experiments ($n = 32$–44). (c) Effects of cdk5/p35 on interaction between syntaxin 1 and APP. N2a cells expressing Venus–syntaxin 1a with cdk5/p35 were used for IP with anti-GFP after cell lysis. Cdk5 reduced the association of Munc18, X11, and APP with syntaxin 1. **, $P < 0.01$.
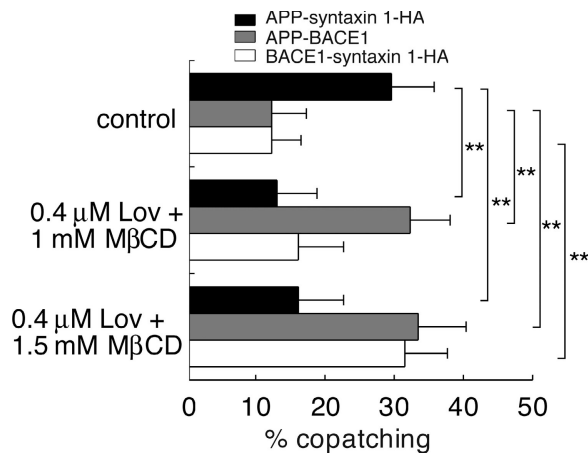
Figure 7. **Effects of cholesterol depletion on microdomain association of APP and segregation between syntaxin 1 and BACE1 in N2a cells.** Mild reduction of cellular cholesterol levels (0.4 µM lovastatin and 1 mM MβCD) caused a switching of APP's microdomain association without changing segregation between BACE1 and syntaxin 1. Further reduction (0.4 µM lovastatin and 1.5 mM MβCD) induced a loss of BACE1 segregation from syntaxin 1, which is consistent with the requirement of intact cholesterol-dependent microdomains for BACE1 exclusion. Data are means + SD based on three independent experiments (n = 31–39). **, $P < 0.01$.

and syntaxin 1 but segregation between APP and BACE1 in a similar way to N2a cells. Cotransfection of p25 caused a shift of APP association from syntaxin 1 to BACE1, suggesting an involvement of microdomain switching in β cleavage promotion by cdk5 in neurons.

Neuronal activity–dependent promotion of β cleavage has been demonstrated (Kamenetz et al., 2003), although the molecular mechanisms have not been elucidated. Most of the current AD mouse models based on the Aβ hypothesis use overexpression of

mutant APP that may induce mislocalization of APP in light of microdomain association. Therefore, we took advantage of an in vitro neuronal hyperactivation model in which neurons expressing endogenous APP are stimulated with picrotoxin (PTX; Kamenetz et al., 2003) or 25 mM KCl (Fig. 9, a–d; Cirrito et al., 2005). To study the effect on APP shedding, C-terminal fragments (CTFs) of APP accumulated by γ-secretase inhibitor treatment were quantified by WB with anti-APPC15. In mature cortical neurons, PTX caused a twofold increase in β/α cleavage ratios (Fig. 9 a), with an increase in p35 levels and without significant changes in BACE1 protein levels or p25/p35 ratios (not depicted). Cdk5 inhibitors roscovitine and olomoucine substantially inhibited the activity-dependent increase in β cleavage, suggesting the involvement of cdk5 in hyperactivity-induced β cleavage. There was a significant difference between roscovitine and olomoucine in efficacy. This may be the result of cdk5-independent potentiation of voltage-dependent Ca^{2+} channels and transmitter release caused by roscovitine (Yan et al., 2002). Effects of cdk5 inhibitors on APP's microdomain association were tested in primary neurons transfected with APP, syntaxin 1–HA, and BACE1AA. Switching of APP's microdomain association from syntaxin 1 to BACE1 was induced by treatment with 25 mM KCl and partly inhibited by roscovitine (Fig. 9 b), which is consistent with the involvement of cdk5-induced microdomain switching in activity-dependent β cleavage promotion.

Thus far, we largely relied on the copatching method using exogenously expressed APP, BACE1AA, and syntaxin 1–HA to show microdomain switching on the cell surface. We tried to obtain biochemical evidence showing a shift in DRM association with endogenous APP in neurons. In DRMs derived from primary neurons treated with the membrane-permeable BACE1 inhibitor, APP was detected in BACE1-containing DRMs after
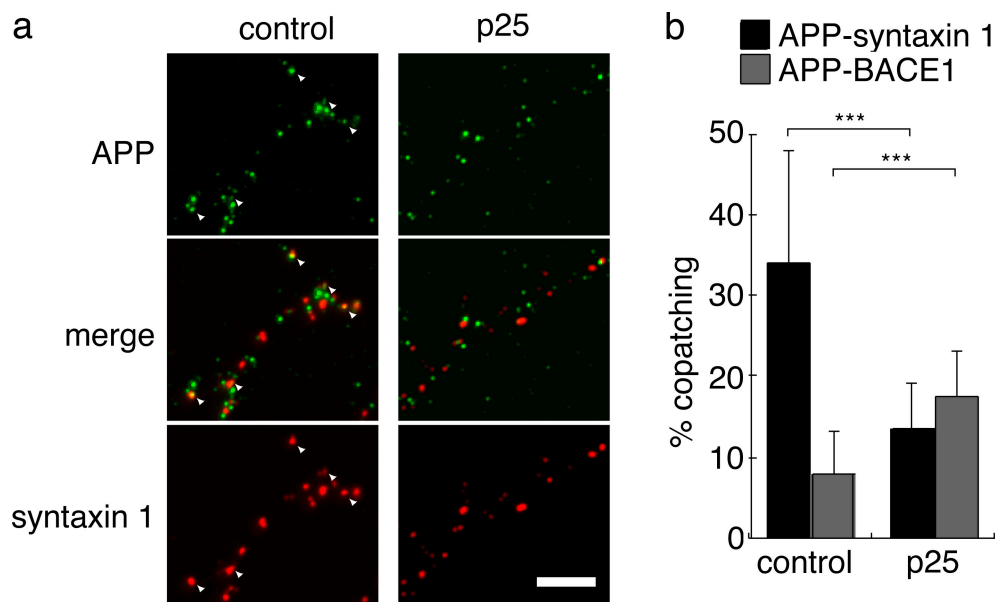
Figure 8. **Overexpression of p25 promotes microdomain switching in primary neurons.** At 3 DIV, hippocampal neurons were transfected with human APP, syntaxin 1–HA, BACE1AA, and p25. At 6 DIV, patch formation was induced by mouse anti–human APPex, rat anti-HA, and rabbit anti-BACE1ex. (a) Coexpression of p25 caused a reduction of APP–syntaxin 1 copatching on axons. Copatching is indicated by arrowheads. Bar, 5 µm. (b) Quantification of copatching on axons demonstrates a cdk5-induced switching of microdomain association of APP in a similar way to N2a cells. Data are means + SD based on three independent experiments (n = 30–38). ***, $P < 0.001$.

long exposures (Fig. 9 c). Association of APP with BACE1-containing DRMs was increased by PTX treatment, and the effect of PTX was inhibited by olomoucine, which is consistent with the switch of APP association indicated by copatching experiments. Finally, we performed copatching experiments of endogenous APP and BACE1 by using chicken anti-BACE1 that induced patch formation of endogenous BACE1 on neurons (Abad-Rodriguez et al., 2004). In hippocampal neurons, copatching between endogenous APP and BACE1 was promoted by 25 mM KCl treatment and partly inhibited by roscovitine (Fig. 9 d). These results are consistent with the involvement of microdomain switching in the activity-dependent promotion of

APP–BACE1 interaction and β cleavage in neurons and suggest cdk5 as a link between microdomain- and activity-dependent regulatory mechanisms of β cleavage.

Discussion

In this study, we have shown a possible regulatory mechanism of APP–BACE1 interaction and β cleavage through switching of APP's association with distinct microdomains. Analysis of APP-rich DRMs suggests the incorporation of APP into cholesterol-dependent protein complexes linked through protein interactions containing X11–Munc18–syntaxin 1, which largely
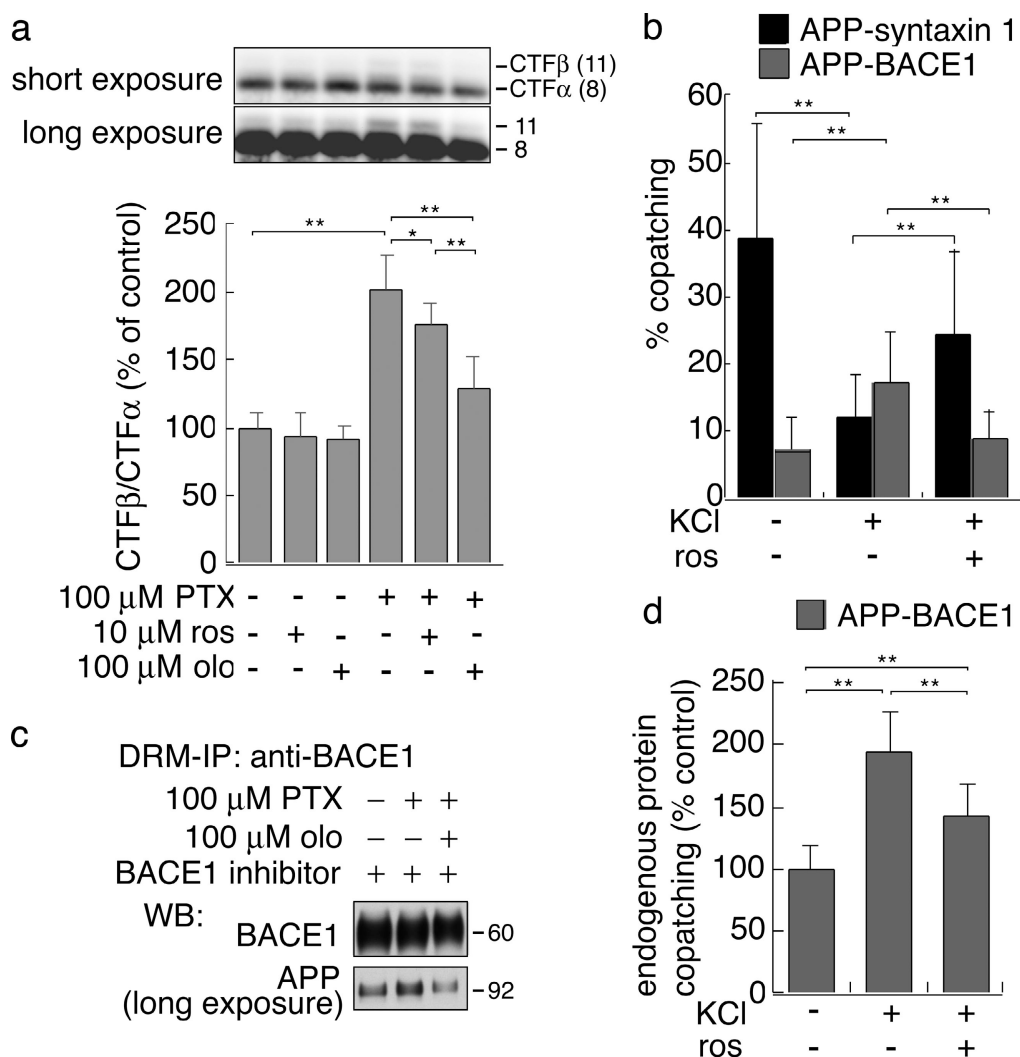
Figure 9. **Cdk5 is implicated in the neuronal activity–dependent promotion of β cleavage and microdomain switching.** (a) Effects of neuronal hyperactivity on β cleavage of endogenous APP. At 11–12 DIV, cortical neurons were treated with PTX and a cdk5 inhibitor in the presence of a γ-secretase inhibitor for 48 h. Accumulated CTFs generated from endogenous APP by α or β cleavage were quantified with anti-APPC15. PTX treatment caused a twofold increase in β cleavage, which was reduced significantly by cdk5 inhibitors. Results are means + SD of 10 measurements. (b) Effects of KCl treatment on microdomain switching. At 3 DIV, hippocampal neurons were transfected with APP, syntaxin 1–HA, and BACE1AA. At 6 DIV, neurons were treated with 25 mM KCl and roscovitine for 20 h. Switching of microdomain association was induced by KCl and substantially inhibited by roscovitine. Data are means + SD based on three independent experiments ($n = 33$–36). (c) A PTX-induced shift of APP association to BACE1-containing DRMs. At 11 DIV, cortical neurons were treated with PTX and olomoucine for 48 h. Before DRM preparation, neurons were treated with the membrane-permeable BACE1 inhibitor for 5 h. DRMs were prepared and used for IP with anti-BACE1c. PTX treatment increased the association of endogenous APP with BACE1-containing DRMs, which was reduced by olomoucine treatment. (d) High K+-induced promotion of copatching of endogenous APP and BACE1 in neurons. At 7–8 DIV, hippocampal neurons were treated with 25 mM KCl and roscovitine for 24 h. Patching of endogenous APP and endogenous BACE1 was induced with rabbit anti-APPex and chicken anti-BACE1ex. A KCl-induced increase in endogenous APP–BACE1 copatching and partial inhibition by roscovitine validated the copatching analysis of exogenously expressed proteins. Data are means + SD based on three independent experiments ($n = 31$ or 32). *, $P < 0.05$; **, $P < 0.01$.

exclude BACE1. Results from copatching experiments indicate the requirement of X11–Munc18 for the association of APP with syntaxin 1 microdomains and for the inhibition of APP–BACE1 interaction. Intriguingly, dissociation of X11–Munc18–syntaxin 1 caused switching of APP's microdomain association from syntaxin 1 microdomains to BACE1-containing microdomains and promotion of β cleavage. From the analyses of primary neurons, this microdomain switching may be involved in neuronal hyperactivity–induced promotion of β cleavage partially through cdk5 activity.

The most commonly used operational criterion for raft association is based on insolubility with Triton X-100 at low temperatures. Although published data clearly demonstrate that APP is not a typical raft resident (Parkin et al., 1999), the application of Lubrol permitted us to show that mature forms of APP are efficiently and consistently recovered in DRMs. Moreover, our procedures minimized mixing of protein components, which allowed us to analyze immunologically isolated DRMs that may reflect the in vivo organization of membrane protein complexes. Cholesterol depletion moves APP, X11, and CASK out of DRMs with less clear changes in Munc18 and syntaxin 1, suggesting that the DRM association of APP partly results from cholesterol-dependent recruitment of APP to syntaxin 1 microdomains containing Munc18 followed by stabilization through X11.

Contrary to our results, one study demonstrated the recovery of APP in Lubrol-soluble fractions (Abad-Rodriguez et al., 2004). We speculate that this discrepancy might be caused by experimental differences. Reduced dissociation of X11–Munc18 in our quickly completed homogenization step may allow the recovery of mature APP in syntaxin 1 DRMs without moving into Lubrol-soluble fractions. Clearly, more needs to be done, but our results might lead to resolution of the discrepancy in DRM association of APP in previous studies (Simons et al., 1998; Parkin et al., 1999; Abad-Rodriguez et al., 2004) by providing a new mode of microdomain association dependent on protein–protein interactions that are easily disrupted by certain DRM preparation methods.

Abad-Rodriguez et al. (2004) demonstrated that a small reduction in cellular cholesterol levels paradoxically enhanced APP–BACE1 interaction and Aβ production. Based on the recovery of APP in non-DRM domains, they proposed the promotion of β cleavage because of the shift of BACE1 localization to non-DRM. Our model provides another mechanism for the promotion of Aβ production from the APP side. Cholesterol reduction inhibits the recruitment of APP and X11 (Fig. S2 b) to the syntaxin 1–containing microdomains and promotes an APP–BACE1 interaction (Fig. 7). Further study is required to clarify whether both nonexclusive mechanisms work together.

Unlike our results, Ehehalt et al. (2003) demonstrated an association of APP with BACE1-containing microdomains on the surface of N2a cells by using copatching experiments. We speculate that they analyzed N2a cells expressing relatively large amounts of exogenous APP (see Materials and methods). APP overexpression will saturate the binding sites and cause mislocalization (Kaether and Haass, 2004), which is similar to the switched conditions to BACE1-containing microdomains in our model. Because microdomain switching mainly relies on the

results of copatching experiments with the endocytosis-defective mutant of BACE1 in this study, the role of microdomain switching in endosomes is speculation. In this respect, their observation might complement ours. They clearly showed a requirement of endocytosis for Aβ production, which was recently confirmed in vivo (Cirrito et al., 2008). Promotion of β cleavage by antibody-induced clustering of APP and BACE1 on the cell surface (Ehehalt et al., 2003) would suggest a critical role of microdomain association during the endocytotic process. Because acidic pH–induced conformational changes in BACE1 may be required for direct APP–BACE1 binding (Shimizu et al., 2008), coresidence of APP and BACE1 in the same microdomains may be a prerequisite for APP–BACE interaction in endosomes. Further studies will be required to clarify the involvement of microdomain association in endosomes in β cleavage.

After exit from the Golgi, APP is primarily transported in axons. From suggested physiological functions, cdk5's effects on APP–BACE1 interaction may be coupled with exo-/endocytosis at presynaptic terminals (Smith and Tsai, 2002) or vesicle formation in the Golgi (Paglini et al., 2001). X11 family proteins are shown to act as coat proteins for sorting and vesicle budding in the TGN to affect APP transport (Hill et al., 2003). This implies that the large APP-containing complex itself is a transport-related structure controlled by X11 for cargo segregation and vesicle packing and by cdk5 for cargo dissociation. In this respect, cholesterol-dependent association of APP with syntaxin 1 microdomains via X11–Munc18 might be related to the sorting events in the TGN and maintained during axonal transport from the TGN through the plasma membrane. However, we cannot exclude the possibility that APP–syntaxin 1 association is formed by a transient X11–Munc18 interaction in the Golgi/TGN that is replaced by other proteins in the post-Golgi vesicles or at the plasma membrane. It is also possible that APP and syntaxin 1 will associate only at the plasma membrane. Further analysis of microdomain association in the TGN and axonal transporting vesicles will be required to clarify the point.

A human brain imaging study indicates a strong correlation between neuronal activity and Aβ deposition (Buckner et al., 2005). Activity-dependent enhancement of β cleavage may be a mechanism underlying this correlation (Kamenetz et al., 2003). Recently, Cirrito et al. (2005, 2008) provided in vivo evidence to show that synaptic activity accelerates Aβ release mainly caused by promotion of APP endocytosis from plasma membrane. Synaptic activity would indirectly promote bulk endocytosis to induce transport of APP and BACE1 into the same endosomal compartment. Our PTX-induced hyperactivation model indicates an involvement of cdk5 in the activity-dependent promotion of β cleavage. We showed a promotion of microdomain switching by cdk5 as one underlying molecular mechanism, but the broad spectrum of cdk5 substrates might indicate that other parallel mechanisms are also involved. Analysis of activity-dependent changes in presynaptic endosomes will be critical to elucidate such molecular mechanisms.

Our data indicate a preferential association of APP with syntaxin 1–containing microdomains via X11–Munc18, which acts as a possible barrier for APP–BACE1 interaction through microdomain segregation. Dissociation of X11–Munc18–syntaxin 1

caused by cdk5 phosphorylation induces a shift of APP association to BACE1-containing microdomains on the cell surface and promotes β cleavage, possibly in endosomes. Our data also implicate cdk5-dependent microdomain switching in the activity-dependent promotion of β cleavage in neurons. Further analyses of the mode and control of APP's microdomain association, especially in presynaptic endosomes, would shed light on the true nature of APP processing in neurons.

Materials and methods

Antibodies
The following antibodies were used: anti-APP (22C11), anti-BACE1, and anti–Thy-1.1 (Millipore); anti-PrP (SAF-32; Cayman Chemical); anti-calnexin, anti-GM130, anti-X11, anti-X11L, anti-CASK, and anti-Munc18 (Transduction Laboratories); anti–Thy-1.2 (AbD Serotec and Invitrogen); anti-X11, anti-p35, and anti-ADAM17 (Santa Cruz Biotechnology, Inc.); rat anti-GFP (RQ2) and mouse anti–syntaxin 1 (HPC-1; MBL International); rabbit anti-Munc18 (Affinity BioReagents); rabbit and mouse anti–syntaxin 1a (Synaptic Systems GmbH); anti-BACE1, anti-sAPPα, and anti-sAPPβ end-specific antibodies (Immuno-Biological Laboratories); rabbit anti–human BACE1 and mouse anti–human APP (P2-1; Invitrogen); mouse anti–human BACE1 (R&D Systems); rabbit and mouse anti-GFP (Invitrogen); rat anti-HA tag (3F10; Roche); mouse anti-HA tag (16B12; Covance); and anti-vesicular stomatitis virus glycoprotein tag ([VSVG] Sigma-Aldrich). For polyclonal antibody production against APP, a bacterially expressed mouse APP extracellular domain (aa 307–591 based on numbering of the 695-aa isoform, APPex), the C-terminal 47 aa of APP (APPc), or the C-terminal 15 aa of APP conjugated with keyhole limpet hemocyanin (APPC15) was injected into rabbits. Antisera were affinity purified with the antigen polypeptide immobilized on Affigel 10 (Bio-Rad Laboratories) or the C-terminal 12-aa peptide on coupling gel (SulfoLink; Thermo Fisher Scientific). To eliminate cross-reaction to amyloid precursor-like proteins (APLPs), APPC15 was adsorbed against corresponding C-terminal peptides of APLP1 and APLP2 and used for WB. Anti-PrP peptide antibodies raised in rabbits (Hashimoto et al., 1992) were purified with immobilized protein A. For production of chicken antibody to the BACE1 extracellular domain, recombinant human BACE1 (aa 14–446) was injected into female chickens. IgY was obtained from eggs laid by a chicken producing patch-inducible antibody with a kit (Thermo Fisher Scientific) and affinity purified with immobilized recombinant BACE1. Rabbit anti-X11 (Santa Cruz Biotechnology, Inc.) was affinity purified with protein A–Sepharose (GE Healthcare) and labeled with biotin (Biotin Labeling Kit-NH$_2$; Dojindo). Biotinylated anti-X11 was detected with HRP mouse antibiotin (Sigma-Aldrich).

Expression constructs
Coding regions of mouse cdk5, p35, and Thy-1.2 were PCR amplified and inserted into pcDNA3.1 (Invitrogen). For PrP expression, a mouse/human hybrid clone of PrP (conjunction at the SmaI site; provided by T. Kitamoto, Tohoku University Graduate School of Medicine, Aoba-ku Sendai, Japan) was amplified and inserted into a pSecTag2 vector (Invitrogen). For rat Munc18-1 and mouse syntaxin 1a, cDNA was cloned using a directional TOPO system (Invitrogen) and transferred to pcDNA-DEST 40 by recombination (Gateway system; Invitrogen). For syntaxin 1–HA, a linker (SGGSGGTGG; Miesenbock et al., 1998) and HA tag were introduced at the C terminus of syntaxin 1a. Expression vectors for truncated mutants of human X11 and N-terminal Venus (an improved version of YFP; provided by A. Miyawaki, RIKEN Brain Science Institute, Wako-shi, Saitama, Japan) fusion protein were made from pcDNA3.1-FLAG-X11 (provided by T. Suzuki, Hokkaido University, Sapporo, Hokkaido, Japan; Araki et al., 2003) as described previously (Mueller et al., 2000). For IP of sAPP in medium, a VSVG tag and pH-dependent version of Venus (pHVenus; Tojima et al., 2007) were inserted at a KpnI site near the N terminus of the human APP695 isoform and in the ectodomain by replacing the Kunitz-type protease inhibitor domain, respectively. Human BACE1 cDNA was provided by A. Takashima (RIKEN Brain Science Institute, Wako-shi, Saitama, Japan). For introduction of the mutations (Munc18 T574A and T574E and BACE1 LL499/500AA), we used a PCR-based method. All constructs were verified by DNA sequencing.

Cell culture and transfection
For DRM preparation, cortical neurons from embryonic day 17 mouse or rat fetuses were prepared by trypsin digestion. Cells were plated on poly-ethyleneimine-coated plastic culture dishes (3 × 10^6 cells per 6-cm dish) and incubated in Neurobasal medium supplemented with B27 (Invitrogen). For inhibition of BACE1 activity, cortical neurons were treated with 1 μM N-[(1S,2R)-1-benzyl-3-(cyclopropylamino)-2-hydroxypropyl]-5-[methyl(methylsulfony)amino]-N'-[(1R)-1-phenylethyl]isophthalamide (EMD; Stachel et al., 2004) for 5 h and used for DRM preparation. For copatching experiments in neurons, mouse embryonic day 18 hippocampal neurons were cultured on polyethyleneimine-coated coverslips. For BACE1 patching, BACE1AA was expressed in neurons except for patching of endogenous BACE1 as shown in Fig. 9 d. N2a cells were maintained in 10% FBS/DME and seeded onto polylysine-coated chamber slides for staining. For copatching experiments, the cells were used after 20–24 h of transfection to avoid overexpression of proteins on the cell surface. For cholesterol depletion in N2a cells, cells were treated with 0.4 μM lovastatin (Sigma-Aldrich) and 1 mM MβCD (Sigma-Aldrich) for mild reduction or 0.4 μM lovastatin and 1.5 mM MβCD for moderate reduction (Abad-Rodriguez et al., 2004) for 20 h at 37°C. Parallel experiments showed a reduction in cellular cholesterol levels to 93.6 ± 8.3% and 77.9 ± 3.8% (percentage of control; n = 3), respectively. For cholesterol depletion or replenishment in cortical neurons, cells were treated with 10 mM MβCD in the medium for 30 min at 37°C or further treated with 0.3 mM of the cholesterol–MβCD complex for 30 min.

DRM preparation
All procedures were performed at 4°C. Frozen mouse or rat brain tissue was homogenized quickly in MES-buffered saline ([MBS] 25 mM MES and 150 mM NaCl, pH 6.5) containing 1% nonionic detergent, Triton X-100, Brij 97 (Sigma-Aldrich), or Lubrol WX (Lubrol 17A17; Serva) and Complete protease inhibitor cocktail (Roche). The homogenate was incubated for 30 min and centrifuged at 2,000 g for 10 min. The supernatant was adjusted to 40% sucrose by adding the same volume of 80% sucrose in MBS and was transferred to 13-ml ultracentrifuge tubes. The sample was overlaid with a 5/10/20/30% discontinuous sucrose gradient in MBS and centrifuged at 260,000 g for 21 h in a rotor (SW-41Ti; Beckman Coulter). We collected 1-ml fractions from the top (total of 12 fractions + precipitation) and stored them at −80°C. From primary cultured embryonic day 17 mouse cortical neurons, DRM fractions were prepared as described previously (Roper et al., 2000) with some modifications. Sucrose flotation was performed in a rotor (SW-55Ti; Beckman Coulter) with the aforementioned gradient, and 12 fractions were taken after centrifugation. The total cholesterol level was measured using a Determiner (TC55; Kyowa Medex) or Amplex Red kit (Invitrogen). GM1-ganglioside was detected by HRP-labeled cholera toxin (Sigma-Aldrich) on blots.

IP of DRMs
All procedures were performed at 4°C. Affinity-purified anti-APP specific to the C-terminal intracellular domain (APPc) or extracellular domain (APPex) or nonimmune rabbit IgG was bound to protein A magnetic beads (Invitrogen). DRMs were diluted with the same volume of 0.1% Lubrol in TBS (25 mM Tris and 150 mM NaCl, pH 8) containing Complete protease inhibitor cocktail. After preclearing, Lubrol DRMs were incubated with antibody-bound beads overnight with gentle mixing. Beads were recovered by magnetic separation and washed four times with TBS containing 0.1% Lubrol WX before being boiled in lithium dodecyl sulfate sample buffer (NuPAGE; Invitrogen). IP of DRMs with anti-BACE1 (Immuno-Biological Laboratories) was performed in the same way.

DRM protein identification
Protein bands of interest were excised from Coomassie brilliant blue–stained gels (NuPAGE system). The proteins were in-gel digested with trypsin, and generated peptides were analyzed by the electrospray ionization liquid chromatography/MS/MS system (LCQ-Deca XP; Thermo Quest). MASCOT software (Matrix Science) was used for predicting the candidate sequence for DRM proteins.

Copatching experiments on N2a cells
Copatching experiments were performed as previously described at 11°C on hippocampal neurons or N2a cells (Harder et al., 1998). For BACE1 patching in N2a cells, we took advantage of a mutant BACE1 lacking a C-terminal endocytosis signal (LL499/500AA, BACE1AA; Pastorino et al., 2002). Initial attempts at copatching of endogenous APP–BACE1 in N2a cells failed because the surface expression of wild-type BACE1 was limited in N2a cells and insufficient for patch formation. Upon transfection, cells expressing enough wild-type BACE1 for patch formation showed almost no staining of FL-APP on the surface, probably because of intracellular β cleavage

of APP during transport to the cell surface. Expression of a very small amount of BACE1AA enabled us to observe patches of BACE1 and APP simultaneously on the surface. This mutant has similar properties to wild-type BACE1 in copatching with Thy-1 and separation from PrP and syntaxin 1. The primary antibodies used were affinity-purified rabbit anti-APPex, mouse anti–human APP, anti-Thy-1.2 (rat or mouse), anti-PrP (mouse or rabbit), anti–human BACE1ex (mouse or rabbit), and anti-HA (rat). After a 1.5-h incubation with primary antibodies in 1 mg/ml BSA in HBSS, patches were induced by a 1-h incubation with goat secondary antibodies labeled with Alexa Fluor 488 or 594 (Invitrogen). To eliminate cross-species reactions, the secondary antibodies were extensively adsorbed against mouse, rabbit, or rat IgG (Jackson ImmunoResearch Laboratories) immobilized on agarose beads. In the case of APP–syntaxin 1, the large and rigid complexes containing APP–X11–Munc18–syntaxin 1 would be cross-linked to APP-free syntaxin 1–Munc18 clusters or SNARE complexes by antibody treatment because of the similar lipid composition in microdomains. Most of the antibody-induced clusters would generate partial overlap through sterically constrained states by the protein complexes. Because complete copatching requires intermiscibility of two molecules on the membrane, we think that the standard copatching measurement is not appropriate in our case. In fact, we observed that most of the patches show partial overlap, which would be estimated as negative by the standard copatching analysis method. Therefore, we used the Metamorph software's colocalization extension (MDS Analytical Technologies) in a pixel-based manner for quantification of copatching. In randomly selected cells, fluorescence images corresponding to the top of the free surface were captured at RT on a microscope (IX70; Olympus) equipped with a cooled charge-coupled device camera (Cool SNAPHQ; Roper Scientific) controlled by Metamorph through a water immersion 60× NA 1.2 objective lens, a 1.5× magnifying lens, and filter sets (86006; Chroma Technology Corp.). An in-focus region of images was selected with a region of interest tool, and area-based measurement of colocalization was performed after automatic background subtraction and segmentation. Because overexpression of proteins on the cell surface caused deleterious effects on copatching like fusion of patches, we used minimal amounts of plasmids for only a small fraction of cells to form patches of both proteins. Thus, we omitted the cells showing patches of only one protein or signs of overexpression from analysis. Data were collected from >10 images per well and at least three independent experiments.

Copatching experiments on primary neurons
For syntaxin 1 and BACE1 patching on axons of primary neurons, 3 days in vitro (DIV) hippocampal neurons were transfected with wild-type human APP, syntaxin 1–HA, and BACE1AA with or without p25. At 6 DIV, living neurons were treated with primary and secondary antibodies for copatching. For neuronal hyperactivity by KCl treatment, the neurons were cultured in medium containing 25 mM KCl for 24 h before copatching experiments in the presence or absence of a cdk5 inhibitor because of insensitivity to PTX in the premature state. A 20-pixel-wide and 500-pixel (∼54 µm)-long region along the axon from the tip was selected, and colocalization was measured in a similar way to the copatching analysis on N2a cells. For copatching of endogenous APP and BACE1, rabbit anti-APPex and chicken anti-BACE1ex were used for 7–8 DIV neurons with or without 24-h KCl treatment. Randomly selected regions were used for measurement of colocalization.

Quantification of sAPP in medium and APP-CTFs in cell lysates
To test the effects of X11 truncated mutants on APP shedding, N2a cells were transfected with a minimal amount of human wild-type APP tagged with VSVG near the N terminus and each construct to be tested. For the sAPP assay, the medium was replaced on the next day. After a 24-h incubation, the medium was harvested and used for IP of released sAPP with anti-VSVG tag (Sigma-Aldrich). In captured sAPP, sAPPα and sAPPβ were detected by WB with anti-sAPPα and anti-sAPPβ end-specific antibodies (Immuno-Biological Laboratories) and quantified. To study the effect of RNAi-mediated Munc18 knockdown on APP shedding, we used human APP in which pHVenus (Tojima et al., 2007) was inserted in the ectodomain and rat anti-GFP (MBL International) for IP. For quantification of CTFs derived from endogenous APP in primary neurons, 11–12 DIV mouse cortical neurons were treated with 1 µM N-[N-(3,5-difluorophenacetyl-L-alanyl)]-(S)-phenylglycine t-butyl ester) for 48 h in the presence or absence of 100 µM PTX with a cdk5 inhibitor. The cells were lysed with 1% SDS in 50 mM Tris, pH 6.8, containing Complete protease inhibitor cocktail and heated at 100°C for 5 min. CTFα and CTFβ were detected by WB with anti-APPC15 and quantified. The identity of the CTFβ band was confirmed by IP of the CTFs followed by WB with anti–mouse Aβ N terminus.

RNAi
For RNAi-mediated knockdown of mouse Munc18-1, we used the artificial micro-RNA system with predesigned target sequences (Block-iT Pol II miR RNAi expression vector; Invitrogen). Among four predesigned sequences, CTGAATGAGATGCGCTGTGCT was the most effective and was used for gene silencing of Munc18-1. For copatching experiments, N2a cells were transfected with microRNA vector and enhanced CFP to mark the transfected cells. After 2 d, N2a cells were transfected again with human APP and syntaxin 1–HA. After 20–24 h, patch formation was induced on N2a cells in which only CFP-positive cells were analyzed.

Electrophoresis and WB
For WB, proteins were resolved by the NuPAGE system and transferred onto polyvinylidene fluoride membranes. After incubation with primary and HRP-labeled secondary antibodies, the blots were developed with ECL solution (GE Healthcare). For quantification, chemiluminescence light signals in SuperSignal Dura or Femto substrate (Thermo Fisher Scientific) were captured by a cooled charge-coupled device camera system (LAS-1000plus; Fuji Film) that ensured wide ranges of linearity. For quantification of proteins, gels were stained with SYPRO Ruby (Invitrogen) according to the manufacturer's instructions. Fluorescence signals were captured in the same cooled charge-coupled device system.

Detergent-free DRM preparation
For the detergent-free method, low density membrane fractions were prepared from primary cultured cortical neurons using Na_2CO_3 as described previously (Song et al., 1996). In brief, the cells were homogenized in 500 mM Na_2CO_3 by passing through a 27-G needle and were briefly sonicated. The homogenate was mixed with the same volume of 90% sucrose in MBS, put at the bottom of a 5.5-ml tube, and overlaid with a 5–35% discontinuous sucrose gradient in MBS containing 250 mM Na_2CO_3. After centrifugation at 250,000 g for 14 h in a rotor (SW55Ti), 0.7-ml fractions were collected from the top (total of eight fractions + precipitation). For IP of membranes prepared in detergent-free conditions, 5 mg/ml BSA was added instead of detergent.

EM
For morphological observation, dialyzed DRM fractions against PBS were adsorbed onto carbon-coated copper grids. The DRMs on grids were fixed with 2% paraformaldehyde and 2% glutaraldehyde in 100 mM sodium phosphate buffer and negatively stained with 2% sodium phosphotungstic acid. Images were recorded on an electron microscope (912AB; LEO Electron Microscopy). For immuno-EM, adsorbed DRMs on grids were incubated with anti-APPc at 4°C overnight and with colloidal gold-conjugated secondary antibody (1:200; GE Healthcare). After fixation with 2% glutaraldehyde, the DRMs on grids were negatively stained and observed on the same microscope. For analysis of distribution of the anti-APP labels, IPLab software (version 3.9; BD Biosciences) was used. On the captured digital images, membrane perimeters were manually traced with segmentation tools, and membrane areas were calculated. On the image, the number of gold particles was counted and assigned to the numbered membrane in the segmented image.

Glycerol gradient ultracentrifugation
Lubrol DRMs derived from brain tissues were treated with 60 mM OG at RT for 30 min and overlaid onto a 15–60% continuous glycerol gradient in 60 mM OG and 10 mM Tris, pH 7.4, with protease inhibitor cocktail. After centrifugation at 100,000 g for 3.5 h in a rotor (SW-55Ti), 300 µl was collected from the top (total of 16 fractions + precipitation). In parallel, the standard proteins Blue Carrier (6,000 kD; Thermo Fisher Scientific) and thyroglobulin (GE Healthcare) were sedimented in the same way. The fractions corresponding to ∼6,000 kD in size were collected, diluted with 60 mM OG in TBS, and used for IP with anti-APPc.

Distribution analysis of fluorescent protein-tagged APP, syntaxin 1–HA, and BACE1AA
N2a cells were transfected with pHVenus-APP, syntaxin 1a–pHVenus-HA, or BACE1AA–enhanced CFP, and signals from fluorescent proteins in live cells were captured by a fluorescence microscope (IX71; Olympus) equipped with a stage incubator (Tokai Hit) set at 37°C. The living cells were sequentially incubated with mouse anti-APPex, rat anti-HA, or rabbit anti-BACE1ex and with Alexa Fluor 594 goat anti–mouse IgG, Alexa Fluor 594 goat anti–rat IgG, or Alexa Fluor 488 goat anti–rabbit IgG at 11°C. Fluorescent signals on unfixed N2a cells derived from fluorescent proteins and secondary antibodies were captured at RT. For capturing images, we

used a cooled charge-coupled device camera (ORCA-AG; Hamamatsu Photonics) controlled by Metamorph, a water immersion 60× NA 1.2 objective lens, a 1.6× magnifying lens, and filter sets (89006; Chroma Technology Corp.).

Statistical analysis

Data are expressed as means ± SD, and error bars represent SD. Statistical analyses were performed by the Tukey-Kramer test for multiple comparisons or by the two-tailed Student's *t* test for two groups; significance was set at *, $P < 0.05$; **, $P < 0.01$; or ***, $P < 0.001$.

Online supplemental material

Fig. S1 shows EM analysis of DRM morphology and APP distribution on DRMs. Fig. S2 shows WB analysis of protein components in large APP-containing complexes in Lubrol DRMs and cholesterol-dependent DRM association of APP and a fraction of X11 and CASK. Fig. S3 shows WB analysis of protein components in APP-containing floating membranes prepared by a detergent-free method. Fig. S4 shows WB analysis of expression levels of syntaxin 1–HA in N2a cells in copatching experiments. Fig. S5 shows patch formation through antibody-induced clustering of cell surface–exposed APP, syntaxin 1–HA, and BACE1 in N2a cells. Online supplemental material is available at http://www.jcb.org/cgi/content/full/jcb.200804075/DC1.

References

Abad-Rodriguez, J., M.D. Ledesma, K. Craessaerts, S. Perga, M. Medina, A. Delacourte, C. Dingwall, B. De Strooper, and C.G. Dotti. 2004. Neuronal membrane cholesterol loss enhances amyloid peptide generation. *J. Cell Biol.* 167:953–960.

Ando, K., K.I. Iijima, J.I. Elliott, Y. Kirino, and T. Suzuki. 2001. Phosphorylation-dependent regulation of the interaction of amyloid precursor protein with Fe65 affects the production of beta-amyloid. *J. Biol. Chem.* 276:40353–40361.

Araki, Y., S. Tomita, H. Yamaguchi, N. Miyagi, A. Sumioka, Y. Kirino, and T. Suzuki. 2003. Novel cadherin-related membrane proteins, Alcadeins, enhance the X11-like protein-mediated stabilization of amyloid beta-protein precursor metabolism. *J. Biol. Chem.* 278:49448–49458.

Borg, J.P., Y. Yang, M. De Taddeo-Borg, B. Margolis, and R.S. Turner. 1998. The X11alpha protein slows cellular amyloid precursor protein processing and reduces Abeta40 and Abeta42 secretion. *J. Biol. Chem.* 273:14761–14766.

Buckner, R.L., A.Z. Snyder, B.J. Shannon, G. LaRossa, R. Sachs, A.F. Fotenos, Y.I. Sheline, W.E. Klunk, C.A. Mathis, J.C. Morris, and M.A. Mintun. 2005. Molecular, structural, and functional characterization of Alzheimer's disease: evidence for a relationship between default activity, amyloid, and memory. *J. Neurosci.* 25:7709–7717.

Cirrito, J.R., K.A. Yamada, M.B. Finn, R.S. Sloviter, K.R. Bales, P.C. May, D.D. Schoepp, S.M. Paul, S. Mennerick, and D.M. Holtzman. 2005. Synaptic activity regulates interstitial fluid amyloid-beta levels in vivo. *Neuron.* 48:913–922.

Cirrito, J.R., J.E. Kang, J. Lee, F.R. Stewart, D.K. Verges, L.M. Silverio, G. Bu, S. Mennerick, and D.M. Holtzman. 2008. Endocytosis is required for synaptic activity-dependent release of amyloid-beta in vivo. *Neuron.* 58:42–51.

Cruz, J.C., D. Kim, L.Y. Moy, M.M. Dobbin, X. Sun, R.T. Bronson, and L.H. Tsai. 2006. p25/cyclin-dependent kinase 5 induces production and intraneuronal accumulation of amyloid beta in vivo. *J. Neurosci.* 26:10536–10541.

De Strooper, B., and W. Annaert. 2000. Proteolytic processing and cell biological functions of the amyloid precursor protein. *J. Cell Sci.* 113:1857–1870.

Ehehalt, R., P. Keller, C. Haass, C. Thiele, and K. Simons. 2003. Amyloidogenic processing of the Alzheimer β-amyloid precursor protein depends on lipid rafts. *J. Cell Biol.* 160:113–123.

Fassbender, K., M. Simons, C. Bergmann, M. Stroick, D. Lutjohann, P. Keller, H. Runz, S. Kuhl, T. Bertsch, K. von Bergmann, et al. 2001. Simvastatin strongly reduces levels of Alzheimer's disease beta-amyloid peptides Abeta 42 and Abeta 40 in vitro and in vivo. *Proc. Natl. Acad. Sci. USA.* 98:5856–5861.

Fletcher, A.I., R. Shuang, D.R. Giovannucci, L. Zhang, M.A. Bittner, and E.L. Stuenkel. 1999. Regulation of exocytosis by cyclin-dependent kinase 5 via phosphorylation of Munc18. *J. Biol. Chem.* 274:4027–4035.

Grimm, M.O., H.S. Grimm, A.J. Patzold, E.G. Zinser, R. Halonen, M. Duering, J.A. Tschape, B.D. Strooper, U. Muller, J. Shen, and T. Hartmann. 2005. Regulation of cholesterol and sphingomyelin metabolism by amyloid-beta and presenilin. *Nat. Cell Biol.* 7:1118–1123.

Harder, T., P. Scheiffele, P. Verkade, and K. Simons. 1998. Lipid domain structure of the plasma membrane revealed by patching of membrane components. *J. Cell Biol.* 141:929–942.

Hashimoto, K., T. Mannen, and N. Nukina. 1992. Immunohistochemical study of kuru plaques using antibodies against synthetic prion protein peptides. *Acta Neuropathol.* 83:613–617.

Hill, K., Y. Li, M. Bennett, M. McKay, X. Zhu, J. Shern, E. Torre, J.J. Lah, A.I. Levey, and R.A. Kahn. 2003. Munc18 interacting proteins: ADP-ribosylation factor-dependent coat proteins that regulate the traffic of beta-Alzheimer's precursor protein. *J. Biol. Chem.* 278:36032–36040.

Ho, A., W. Morishita, R.E. Hammer, R.C. Malenka, and T.C. Sudhof. 2003. A role for Mints in transmitter release: Mint 1 knockout mice exhibit impaired GABAergic synaptic transmission. *Proc. Natl. Acad. Sci. USA.* 100:1409–1414.

Ho, C.S., V. Marinescu, M.L. Steinhilb, J.R. Gaut, R.S. Turner, and E.L. Stuenkel. 2002. Synergistic effects of Munc18a and X11 proteins on amyloid precursor protein metabolism. *J. Biol. Chem.* 277:27021–27028.

Iijima, K., K. Ando, S. Takeda, Y. Satoh, T. Seki, S. Itohara, P. Greengard, Y. Kirino, A.C. Nairn, and T. Suzuki. 2000. Neuron-specific phosphorylation of Alzheimer's beta-amyloid precursor protein by cyclin-dependent kinase 5. *J. Neurochem.* 75:1085–1091.

Kaether, C., and C. Haass. 2004. A lipid boundary separates APP and secretases and limits amyloid β-peptide generation. *J. Cell Biol.* 167:809–812.

Kamenetz, F., T. Tomita, H. Hsieh, G. Seabrook, D. Borchelt, T. Iwatsubo, S. Sisodia, and R. Malinow. 2003. APP processing and synaptic function. *Neuron.* 37:925–937.

King, G.D., and R.S. Turner. 2004. Adaptor protein interactions: modulators of amyloid precursor protein metabolism and Alzheimer's disease risk? *Exp. Neurol.* 185:208–219.

Kojro, E., G. Gimpl, S. Lammich, W. Marz, and F. Fahrenholz. 2001. Low cholesterol stimulates the nonamyloidogenic pathway by its effect on the alpha-secretase ADAM 10. *Proc. Natl. Acad. Sci. USA.* 98:5815–5820.

Lang, T., D. Bruns, D. Wenzel, D. Riedel, P. Holroyd, C. Thiele, and R. Jahn. 2001. SNAREs are concentrated in cholesterol-dependent clusters that define docking and fusion sites for exocytosis. *EMBO J.* 20:2202–2213.

Liu, J., S.A. Ernst, S.E. Gladycheva, Y.Y. Lee, S.I. Lentz, C.S. Ho, Q. Li, and E.L. Stuenkel. 2004. Fluorescence resonance energy transfer reports properties of syntaxin1a interaction with Munc18-1 in vivo. *J. Biol. Chem.* 279:55924–55936.

Madore, N., K.L. Smith, C.H. Graham, A. Jen, K. Brady, S. Hall, and R. Morris. 1999. Functionally different GPI proteins are organized in different domains on the neuronal surface. *EMBO J.* 18:6917–6926.

Miesenbock, G., D.A. De Angelis, and J.E. Rothman. 1998. Visualizing secretion and synaptic transmission with pH-sensitive green fluorescent proteins. *Nature.* 394:192–195.

Mitchell, S.J., and T.A. Ryan. 2004. Syntaxin-1A is excluded from recycling synaptic vesicles at nerve terminals. *J. Neurosci.* 24:4884–4888.

Mueller, H.T., J.P. Borg, B. Margolis, and R.S. Turner. 2000. Modulation of amyloid precursor protein metabolism by X11alpha /Mint-1. A deletion analysis of protein-protein interaction domains. *J. Biol. Chem.* 275:39302–39306.

Nguyen, M.D., W.E. Mushynski, and J.P. Julien. 2002. Cycling at the interface between neurodevelopment and neurodegeneration. *Cell Death Differ.* 9:1294–1306.

Nixon, R.A. 2005. Endosome function and dysfunction in Alzheimer's disease and other neurodegenerative diseases. *Neurobiol. Aging.* 26:373–382.

Paglini, G., L. Peris, J. Diez-Guerra, S. Quiroga, and A. Caceres. 2001. The Cdk5-p35 kinase associates with the Golgi apparatus and regulates membrane traffic. *EMBO Rep.* 2:1139–1144.

Parkin, E.T., A.J. Turner, and N.M. Hooper. 1999. Amyloid precursor protein, although partially detergent-insoluble in mouse cerebral cortex, behaves as an atypical lipid raft protein. *Biochem. J.* 344:23–30.

Pastorino, L., A.F. Ikin, A.C. Nairn, A. Pursnani, and J.D. Buxbaum. 2002. The carboxyl-terminus of BACE contains a sorting signal that regulates BACE trafficking but not the formation of total A(beta). *Mol. Cell. Neurosci.* 19:175–185.

Pike, L.J. 2004. Lipid rafts: heterogeneity on the high seas. *Biochem. J.* 378:281–292.

Refolo, L.M., B. Malester, J. LaFrancois, T. Bryant-Thomas, R. Wang, G.S. Tint, K. Sambamurti, K. Duff, and M.A. Pappolla. 2000. Hypercholesterolemia accelerates the Alzheimer's amyloid pathology in a transgenic mouse model. *Neurobiol. Dis.* 7:321–331.

Reinhard, C., S.S. Hebert, and B. De Strooper. 2005. The amyloid-beta precursor protein: integrating structure with biological function. *EMBO J.* 24:3996–4006.

Riddell, D.R., G. Christie, I. Hussain, and C. Dingwall. 2001. Compartmentalization of beta-secretase (Asp2) into low-buoyant density, noncaveolar lipid rafts. *Curr. Biol.* 11:1288–1293.

Rizo, J., and T.C. Sudhof. 2002. SNAREs and Munc18 in synaptic vesicle fusion. *Nat. Rev. Neurosci.* 3:641–653.

Roper, K., D. Corbeil, and W.B. Huttner. 2000. Retention of prominin in microvilli reveals distinct cholesterol-based lipid micro-domains in the apical plasma membrane. *Nat. Cell Biol.* 2:582–592.

Sano, Y., T. Nakaya, S. Pedrini, S. Takeda, K. Iijima-Ando, K. Iijima, P.M. Mathews, S. Itohara, S. Gandy, and T. Suzuki. 2006. Physiological mouse brain Abeta levels are not related to the phosphorylation state of threonine-668 of Alzheimer's APP. *PLoS ONE.* 1:e51.

Selkoe, D.J., and D. Schenk. 2003. Alzheimer's disease: molecular understanding predicts amyloid-based therapeutics. *Annu. Rev. Pharmacol. Toxicol.* 43:545–584.

Shimizu, H., A. Tosaki, K. Kaneko, T. Hisano, T. Sakurai, and N. Nukina. 2008. Crystal structure of an active form of BACE1, an enzyme responsible for amyloid beta protein production. *Mol. Cell. Biol.* 28:3663–3671.

Simons, K., and D. Toomre. 2000. Lipid rafts and signal transduction. *Nat. Rev. Mol. Cell Biol.* 1:31–39.

Simons, M., P. Keller, B. De Strooper, K. Beyreuther, C.G. Dotti, and K. Simons. 1998. Cholesterol depletion inhibits the generation of beta-amyloid in hippocampal neurons. *Proc. Natl. Acad. Sci. USA.* 95:6460–6464.

Smith, D.S., and L.H. Tsai. 2002. Cdk5 behind the wheel: a role in trafficking and transport? *Trends Cell Biol.* 12:28–36.

Song, K.S., S. Li, T. Okamoto, L.A. Quilliam, M. Sargiacomo, and M.P. Lisanti. 1996. Co-purification and direct interaction of Ras with caveolin, an integral membrane protein of caveolae microdomains. Detergent-free purification of caveolae microdomains. *J. Biol. Chem.* 271:9690–9697.

Stachel, S.J., C.A. Coburn, T.G. Steele, K.G. Jones, E.F. Loutzenhiser, A.R. Gregro, H.A. Rajapakse, M.T. Lai, M.C. Crouthamel, M. Xu, et al. 2004. Structure-based design of potent and selective cell-permeable inhibitors of human beta-secretase (BACE-1). *J. Med. Chem.* 47:6447–6450.

Tojima, T., H. Akiyama, R. Itofusa, Y. Li, H. Katayama, A. Miyawaki, and H. Kamiguchi. 2007. Attractive axon guidance involves asymmetric membrane transport and exocytosis in the growth cone. *Nat. Neurosci.* 10:58–66.

Vassar, R., B.D. Bennett, S. Babu-Khan, S. Kahn, E.A. Mendiaz, P. Denis, D.B. Teplow, S. Ross, P. Amarante, R. Loeloff, et al. 1999. Beta-secretase cleavage of Alzheimer's amyloid precursor protein by the transmembrane aspartic protease BACE. *Science.* 286:735–741.

Vetrivel, K.S., H. Cheng, W. Lin, T. Sakurai, T. Li, N. Nukina, P.C. Wong, H. Xu, and G. Thinakaran. 2004. Association of gamma-secretase with lipid rafts in post-Golgi and endosome membranes. *J. Biol. Chem.* 279:44945–44954.

Wen, Y., W.H. Yu, B. Maloney, J. Bailey, J. Ma, I. Marie, T. Maurin, L. Wang, H. Figueroa, M. Herman, et al. 2008. Transcriptional regulation of beta-secretase by p25/cdk5 leads to enhanced amyloidogenic processing. *Neuron.* 57:680–690.

Wolozin, B. 2001. A fluid connection: cholesterol and Abeta. *Proc. Natl. Acad. Sci. USA.* 98:5371–5373.

Xie, Z., D.M. Romano, and R.E. Tanzi. 2005. RNA interference-mediated silencing of X11alpha and X11beta attenuates amyloid beta-protein levels via differential effects on beta-amyloid precursor protein processing. *J. Biol. Chem.* 280:15413–15421.

Yan, Z., P. Chi, J.A. Bibb, T.A. Ryan, and P. Greengard. 2002. Roscovitine: a novel regulator of P/Q-type calcium channels and transmitter release in central neurons. *J. Physiol.* 540:761–770.